TESLA-FEL 2003-04

Waveguide Monitors - a New Type of Beam Position Monitors for the TTF FEL

U. Hahn[1], T. Kamps[2], R. Lorenz[3], W.Riesch[4]
H.J. Schreiber[4] and F. Tonisch[4]

[1] DESY Hamburg, 22607 Hamburg, FRG

[2] Royal Holloway University of London, Egham, Surrey, TW20 OEX, United Kingdom

[3] Westdeutscher Rundfunk, 50600 Köln, FRG

[4] DESY Zeuthen, 15735 Zeuthen, FRG

Abstract

The operation of a Free Electron Laser (FEL) at the TESLA Test Facilty (TTF) requires the electron trajectory to be aligned with precision of few micrometer in overlap with the photon beam. To achieve this goal precise position monitoring of the electron beam in the narrow undulator gap is mandatory. A beam position monitor based on a new microwave concept was designed, built and tested in order to avoid possible sparking problems of pick-up monitors. It consists of four ridged waveguides which couple by small slots to the magnetic field of the electron beam. The paper reports the concept, the design and tests of prototypes in a test bench in the laboratory and with beam. TTF FEL measurement results are also presented and possible improvements are discussed.

1 Introduction

In 1995 an international collaboration proposed the construction of the superconducting accelerator of the TESLA Test Facility (TTF) with an integrated Free Electron Laser (FEL) at the Deutsches Elektronensynchrotron DESY in Hamburg [1]. This facility was set-up, commissioned and brought into operation [2]. First lasing of the FEL was observed in 2000 [3].

The operation of a Free Electron Laser in the Self Amplified Spontaneous Emmission mode (SASE) requires the electron trajectories to be aligned with very high precision in overlap with the photon beam. Simulations showed that the mean variation between the photon path (mainly defined by the undulator axis) and the electron trajectory must be kept below 20 μm in order to reach saturation in the undulator [4]. To ensure this overlap, the undulator modules of the TTF FEL were equipped with beam position monitors and steering coils integrated in the undulator vacuum chamber. Pick-up monitors were installed into the first two modules, while the third one was equipped with a new type of waveguide beam position monitors (BPM) to measure the beam position with high resolution in a non-destructive manner in a high radiation enviroment.

In this paper we present the waveguide BPM in its various stages of the development. The mechanical design was essentially predetermined by the small undulator gap of 12 mm, the layout of the vacuum chamber with its cross section of 11.5×128 mm^2, and the undulator magnets, which allowed only for horizontal access. The shape of the waveguides was designed to fit into the vacuum chamber and to realize an effective coupling to the electron beam. Prototypes were constructed and tested in the laboratory and with beam. The results obtained in each development stage will be presented. Finally, the third TTF FEL undulator chamber was equiped with waveguide monitors and data taking started. Problems which were observed at different stages of the monitor development and solutions will also be discussed in the paper.

2 Design and Basic Characteristics of the Waveguide Monitor

Basic mechanical design parameters of the waveguide monitor are determined by their position within the small undulator gap of 12 mm, with only horizontal access. The BPMs have to be an integrated part of the vacuum chamber, taking also into account the beam pipe with 9.5 mm inner diameter. Thus, a compact design is one essential demand for the mechanical realization of the BPMs. The shape of the waveguides is designed in a way which reduces the size and realizes at the same time an effective coupling to the beam field. At the end of each waveguide, a coaxial adapter with a vacuum feedtrough is flange mounted.

The principle design of this new BPM type is sketched in Fig. 1. By four slots[1] a fractional part of the electromagnetic beam field is coupled into special ridge waveguides arranged symmetrically around the beam pipe. Due to restricted vertical space, two waveguide pairs (S1-S3 and S2-S4) were separated by ∼40 mm in beam direction. Each waveguide is inclined by about 35^o with respect to the horizontal axis to achieve highest possible vertical separation of the coupling slots. The size and position of the slots enable a sufficient coupling (about 1%) to the beam field.

As the electric field of the passing electron beam is only transverse to the coupling slots, a coupling to the magnetic field is intended, see Fig. 2. Designing the waveguides the coupling slots of the BPMs can be regarded as a radiating magnet dipole oriented parallel to the magnetic field lines of the passing beam. The aim of the T-ridged waveguide is to generate a lossless transport of the induced electromagnetic field to a matching section. Here, the wave is transferred to a 50 Ω coaxial vacuum feedthrough to leave the vacuum chamber.

[1]Dimensions of these slots are 3.2 × 3.2 mm^2, with a depth of 0.3 mm.

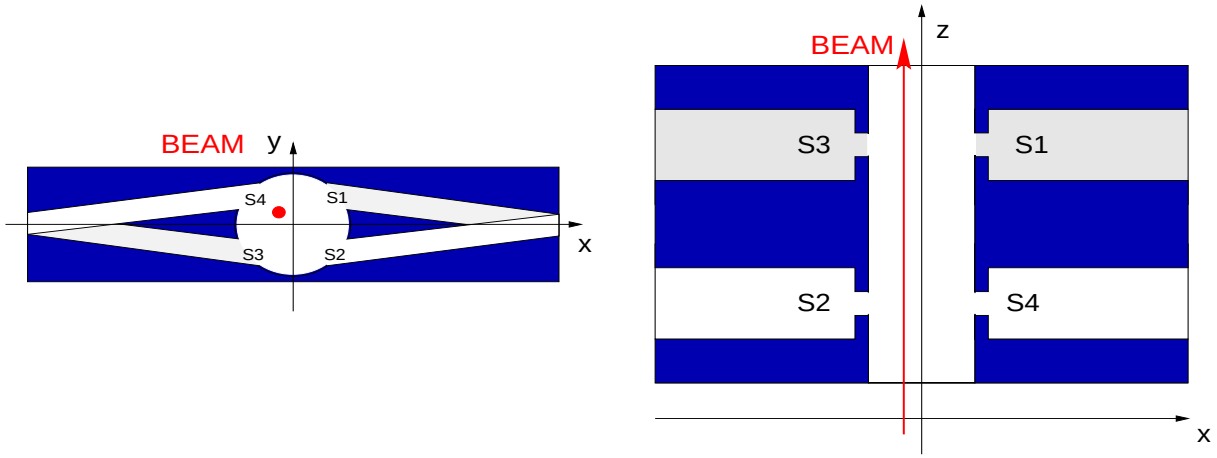

Figure 1: Schematics of the waveguide BPM with four channels and four coupling slots (profile and top view).

An improved version of the monitor (Prototype II) was designed as an integral part of the vacuum chamber[2]. Fig. 3 shows the total view of this version and a view onto its side front with the two waveguide ports and the tapped holes for mounting the vacuum feedthrough. It also shows the waveguide profile and the position of the slots. The electron beam passes the flat chamber through the vacuum flanges at the ends of the prototype. This design provides a better broadband transition between waveguide and vacuum feedthrough. The electrical contact between the ridge and the rectangular block was achieved by means of a $\lambda/4$-transformer produced in one step together with the waveguide ridge structure (see also Fig. 2). The coaxial vacuum feedthrough is connected directly to the socket of the inner transformer block of the T-ridged structure of the waveguide. This technique provides good electrical contact as well as correct positioning and vacuum tight mounting of the elements [5]. Prototype II also achieved a smaller quality factor and consequently less coupling amplitude variation. The waveguide structures were fabricated using Electrical Discharge Machining (EDM).

Detailed MAFIA [6] simulations were performed in order to obtain optimized parameters for coupling slots and transition to the vacuum feedthrough. For more details on design parameters and their variation within reasonable limits obtained from simulations and analytical estimations we refer to [7].

The upper operation working frequency of the waveguide f_w is in principle only limited by the cut-off frequency of the beam pipe with $f_{pipe} = 17.94$ GHz. For $f_w \geq f_{pipe}$, fields generated by interaction between the beam and its surrounding material can couple into the waveguide and might lead to interferences with the signal from the beam. The waveguide working frequency was designed to be 12 GHz. This is mainly due to use of commercially available signal processing components as well as to be sufficiently above the waveguide fundamental cut-off frequency at 8.99 GHz and below 13.24 GHz of its next higher order mode.

When the electrons pass the undulator beam pipe wakefields are generated which can introduce an additional energy spread in the electron bunch and, in turn, might influence SASE. The impact of the waveguide BPMs has been estimated with the result that the overall beam spread

[2]For the first prototype (Prototype I), the inner part of the waveguide ridge was an integrated part of the vacuum flange. This part was inserted into the rectangular waveguide structure which was machined into the vacuum chamber forming the T-ridged waveguide. The antenna has been welded perpendicular to the waveguide with high precision. Due to machining tolerances the electrical contact between the inner part of the ridge and the vacuum chamber wall could not be guaranteed to form a perfect waveguide. The manufacturing process turned out to be complicated and not well suited for mass production of monitors.

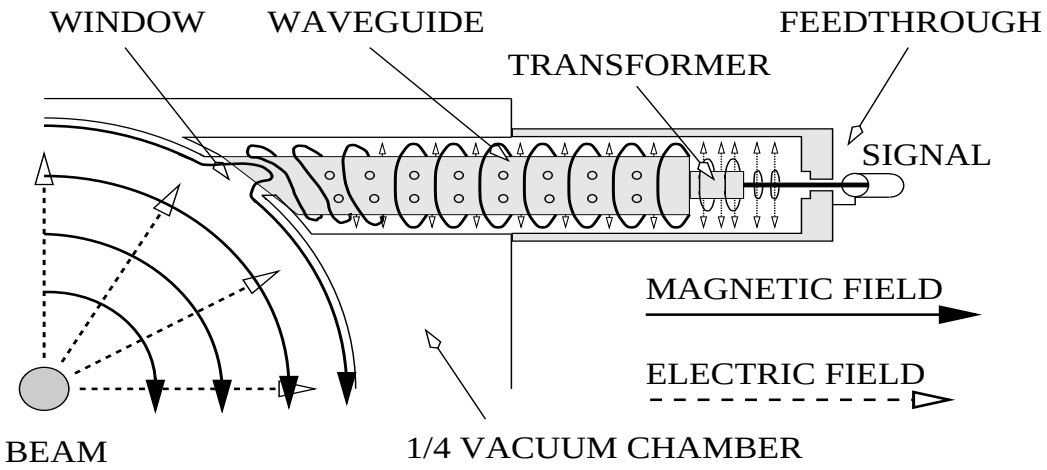

Figure 2: Sketch of the coupling mechanism of the Prototype II monitor.

due to wakefields is tolerable for TTF FEL phase I operation [7], [8].

3 Measurements in the Laboratory

Laboratory measurements of new beam diagnostics elements are useful to confirm basic predictions of simulations and to study specific characteristics under idealized conditions. Also, calibration algorithms might be developed and easily tested at early stages of a device. In our case, broadband measurements were performed to check matching stages, to observe cut-off frequencies and to look for trapped resonances in the waveguides.

For test measurements a set-up as shown in Fig. 4 was constructed and built, with schematics of its electrical facet as shown in Fig. 5.

The electromagnetic field propagating with a relativistic electron beam is similar to the TEM-mode of a coaxial system (see Fig. 2). Such a system has been emulated by placing a stretched copper-beryllium wire of 250 μm diameter inside the BPM. At the input, an impedance transformer was inserted in order to minimize reflections of the electromagnetic wave. At the end of the setup structure, the electromagnetic power had to be damped by an absorber to prevent standing waves by reflections inside the BPM chamber.

Generation of signals with 1 ps bunch length and a charge of 1 nC could not be realized with a pulse generator for prototype tests. Instead, frequency domain measurements up to 16 GHz were performed using a network analyzer. For monitor parameter measurements, a signal generator delivering a 12 GHz continuous wave with 14.8 dBm was in use.

To avoid high frequency oscillations from a moving wire, the BPM itself was moved with respect to the wire by two (x,y) stepping motors, with a position repeatibility of better than 1 μm. Detailed studies were performed for RF input and output ports to provide electrical contact, correct impedance matching and best absorption at the output side as well as to minimize signal losses [7].

Output ports of the prototype were connected via low-loss cables to the electronics. Here, signals exited in the waveguides were filtered at 12 GHz with a bandwith of 730 MHz and then amplified by 20 dB. Since the signal detecting powermeter had only two ports, the signals had to pass a relay cascade. The powermeter was read out by a PC running a LABVIEW data

Figure 3: Photo of Prototype II. top: total view, bottom: view onto sidefront with two waveguide ports and the tapped holes for mounting to the vacuum feedthroughs.

aquisition application via an IEEE 488 interface. The application program also controlled the stepping motor and accounted for the stepping motor movements.

3.1 Transfer Characteristics

The transfer characteristics for each BPM channel were studied with the wire test bench by measuring the S_{21} transmission parameter for a frequency range from 50 MHz to 16 GHz using a network analyser. Our set-up allowed to analyse cut-off frequencies of a waveguide in the frequency range selected. As an example, Fig. 6 shows transfer characteristics for one channel of Prototype I. The transmission is rather small until the waveguide cut-off frequency of about 9 GHz is reached. Above this value, the transmission rises to -42 dB (with respect to the input signal), which corresponds to a coupling amplitude of about 0.8%.

The high-pass characteristics observed were found basically for all channels with acceptable differences due to imperfect mechanical manufacturing of the monitor[3]. For this reason and electrical contact problems as well as a larger broadband transition between the waveguide and

[3]In particular, welding the antenna with very high precision perpendicular to the waveguide at the $\lambda_w/4$ distance turned out to be difficult.

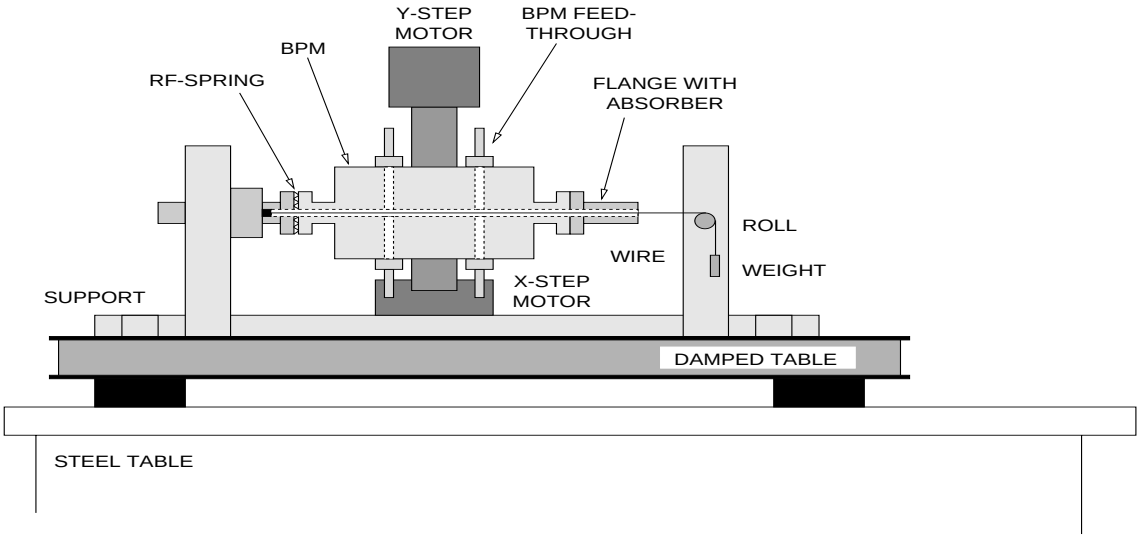

Figure 4: Schematics of the mechanical facet of the laboratory test bench.

the vacuum feedthrough for Prototype II, we present mainly results from Prototype II in the following discussions.

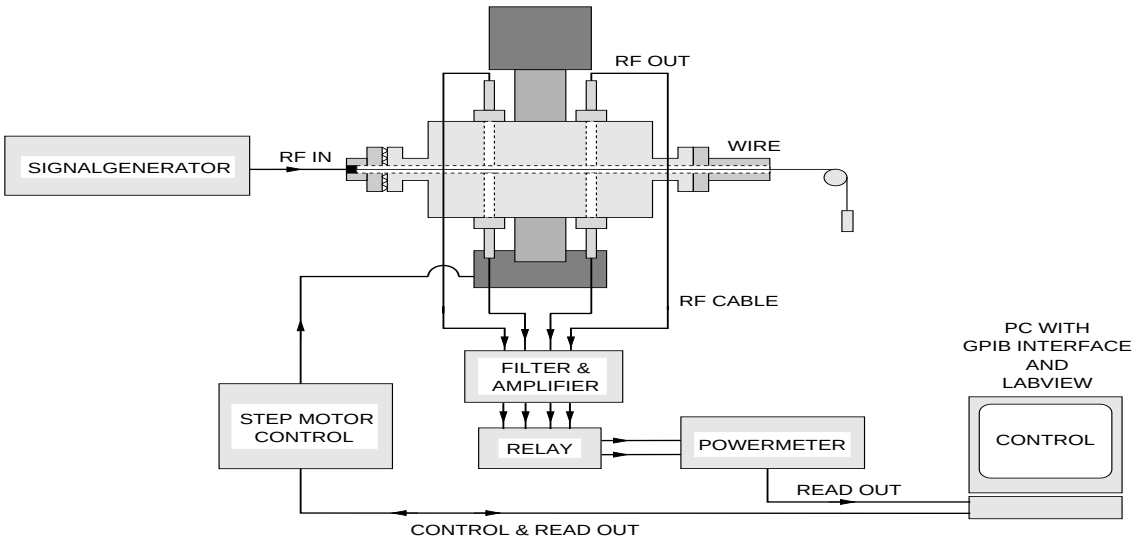

Figure 5: Schematics of the electrical facet of the laboratory test bench.

3.2 Gain

The gain factor is described by the difference between a real and an ideal BPM channel. This factor summarizes all mechanical imperfections and imbalances among the four channels of one monitor unit. Its determination is important for monitor calibration procedures.

Measurements of gain (and sensitivity as discusssed in Section 3.3) were performed with Prototype II mounted on the wire test bench. Cross scan measurements around the center of the monitor as indicated in Fig. 7 were performed, with a typical range of 1 to 2 mm in steps of $\geq$10 μm.

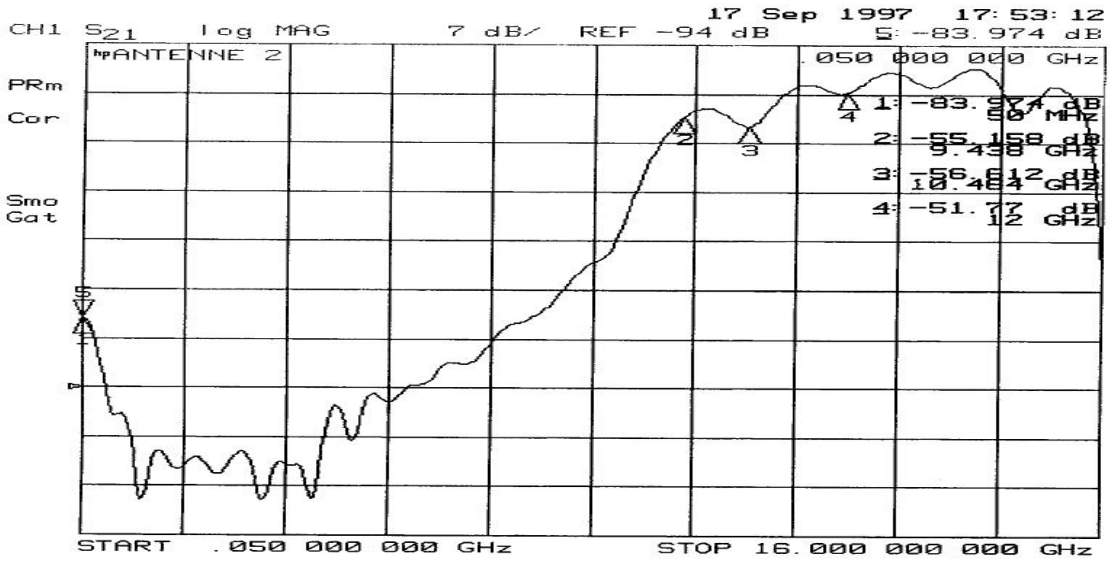

Figure 6: S_{21} parameter of one channel of the Prototype I monitor.

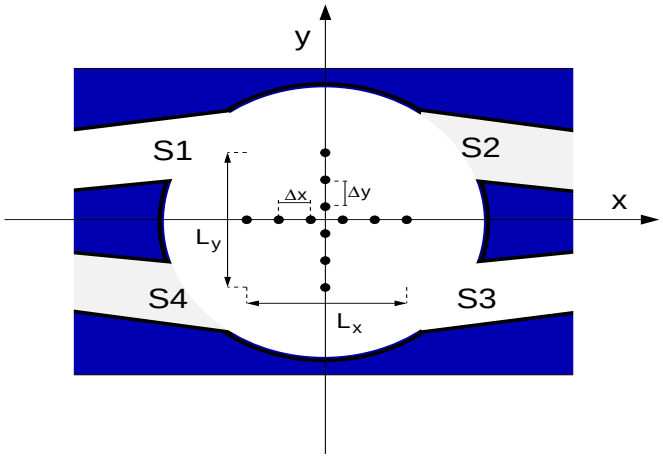

Figure 7: Schematics of the array for cross scan measurements.

The response of an ideal BPM channel i can be calculated using the image charge model [9]

$$S_i = \frac{b^2 - r^2}{b^2 + r^2 - 2br\cos(\phi_i - \theta)} \tag{1}$$

for a slot at (b, ϕ_i) and a beam at position (r, θ). Due to individual transfer characterstics of each channel the measured voltage depends on the response function S_i modified with the channel gain: $V_i = q \cdot g_i \cdot S_i$. Here, q is the factor describing the amplitude of an input signal. Hence the gain of one particular channel is the inverse transmission parameter at 12 GHz normalized to the amplitude induced for a centered wire.

Gain parameters were estimated by measuring the induced voltages $V_{i,j}$ (i=1...4) for j = 1...n wire positions in the BPM aperture. A fit to the image charge model $M_{i,j}$ provides the coupling factor for each channel:

$$M_{i,j} \quad = \quad g_i \cdot \frac{b^2 - r_j^2}{b^2 + r_j^2 - 2br_j\cos\left(\phi_i - \theta_j\right)} \equiv M(i, j; \mathbf{a})$$

$$
\begin{aligned}
& i = 1 \cdots 4 \qquad \text{and} \qquad j = 1 \cdots m \\
\mathbf{a} \;&=\; (g_1, g_2, g_3, g_4),
\end{aligned}
$$

where $\mathbf{a}$ is the array of fitting parameters to be determined.

The waveguide signals were filtered, amplified and measured by means of a powermeter monitored by a PC. In order to exclude effects from imbalances among amplifiers, cables and filters, detected voltages were divided by their amplification factor. The gain results obtained normalized to $g_1 = 1$ are listed in Tab. 1.

Channel	Gain	Slot angle [deg]
1	1.0000 ± 0.0018	35.94 ± 0.13
2	0.9054 ± 0.0017	33.46 ± 0.09
3	1.0668 ± 0.0017	35.92 ± 0.14
4	1.0094 ± 0.0019	34.20 ± 0.13

Table 1: Gain values normalized to g_1=1 and coupling slot angles as derived from a fit to the image charge model.

The gain results are close to the design value with a small root-mean-square spread. This encouraging result compared to Prototype I measurements [7] was mainly due to the broadband matching which reduced the amplitude for trapped modes significantly.

The image charge model was also used to estimate the angles of the coupling slots by including the gain factors as obtained in the previous step. The results of the fit are also given in Tab. 1 and reveal fair agreement with the design value of 35.51^0 (with respect to the x-axis). Slight systematic differences can be accounted for by a small tilt between the BPM reference frame and the test bench system.

3.3 Sensitivity

The sensitivity describes the change of an induced signal amplitude for a given beam off-set. The induced voltages of channel 1 to 4, normalized with corresponding amplifications and damping factors, were used to construct virtual signal functions $L = S_1 + S_4$ and $R = S_2 + S_3$ for the horizontal ($U = S_1 + S_2$ and $D = S_3 + S_4$ for the vertical) direction, see also Fig. 7. The sensitivity S_x (S_y) for the horizontal (vertical) direction is then defined as the slope between set position in x (or y) and the logarithmic ratio of L and R (or U and D)

$$
x \cdot S_x = 20 \cdot \log\left(\frac{L}{R}\right) \qquad \text{and} \qquad y \cdot S_y = 20 \cdot \log\left(\frac{U}{D}\right) \tag{2}
$$

In Fig. 8 values for log-ratios are plotted as function of the wire position. A linear performance for $|x|, |y| \leq 500$ μm around the BPM center can be observed for both prototypes. The moderately improved sensitivity in x might be caused by differences in the slot positions within the monitor.

The resulting sensitivities are listed in Tab. 2, together with results from MAFIA S-Parameter computations and from the image charge model. Good agreement between test bench measurements and expected values is noted.

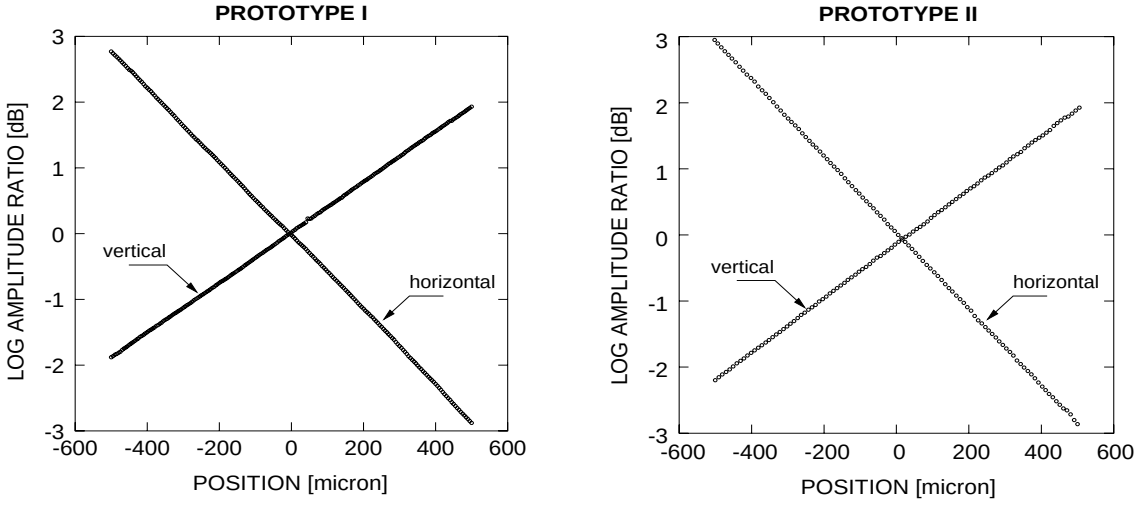

Figure 8: Sensitivity plots for both prototypes.

	Measurements	Simulation	Model
S_x [dB/mm]	5.79 ± 0.04	5.78	5.78
S_y [dB/mm]	4.10 ± 0.04	3.88	4.10

Table 2: Sensitivities as derived from measurements on the wire test bench, MAFIA simulations and the image charge model.

4 Prototype Measurements with Beam

Encouraged by the positive results obtained from laboratory test bench studies, measurements under real beam conditions were considered as an experimental proof of the operation principle of the waveguide monitor. In particular, the coupling of the BPM to a beam field at 12 GHz was measured and compared with test bench results as well as calculations. Basic signal processing electronics using commercially available components were successfully tested.

First beam test data were obtained with Prototype I at the CLIC Test Facility at CERN [10]. Measurements of the four coupling amplitudes were found to be consistent with laboratory test bench measurements. Results on sensitivities in x and y directions were in accord with test bench data and MAFIA simulations [7], too.

Prototype II was installed in the S-Band Test Facility at DESY (SBTF) [11] in a drift region between two quadrupole triplets as illustrated in Fig. 9. Typical SBTF beam parameters relevant for the measurements are summarized in Table 3.

The electron beam with desired time structure and energy was generated and accelerated by three sections. The waveguide monitor has been installed at a location where the beam envelope should be equal for the horizontal and vertical planes. To move the monitor in well-defined steps perpendicular to the beam, a two-dimensional stepping motor frame with the BPM integrated was computer controlled to enable this movement.

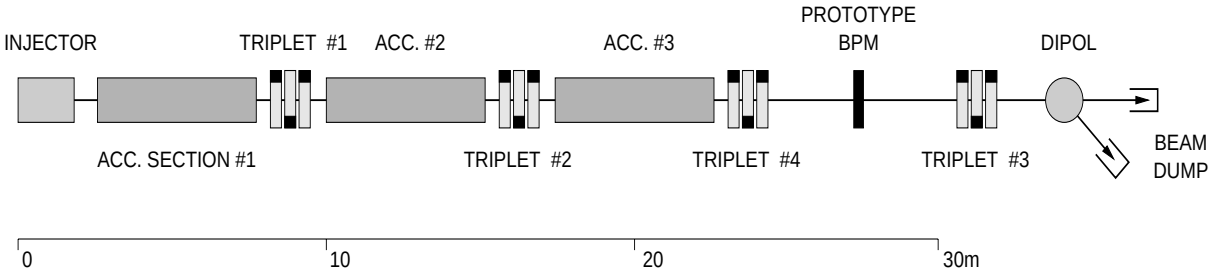

Figure 9: Layout of the S-Band Test Facility with the indicated location of the waveguide BPM Prototype II.

Energy	E	46.7 MeV
Repetition rate	f_r	1 Hz
Bunch charge	q	0.2 nC
Bunch length	σ_z	$4 \cdots 5$ mm
Bunch size	$\sigma_{x,y}$	~ 1 mm

Table 3: S-Band Test Facility beam parameters during measurements.

After centering the beam with quadrupole scans, first measurements were performed by displaying beam induced signals on a digital sampling scope. For the scope trigger, a beam related signal was taken from a stripline BPM in the second quadrupole triplet, including a proper delay of the signal. Unwanted frequencies were filtered before the oscilloscope input. With this set-up, 12 GHz components of beam related induced signals were clearly visible. In a next step, down-converted monitor signals for all four channels were recorded. Down-conversion from 12 GHz was realized using a RF mixer. The needed 12 GHz LO signal with constant amplitude and phase locked to the beam was derived using the 4th harmonic of the accelerating frequency (2.99 GHz), induced in the stripline BPM. After filtering, the remaining IF signal was amplified to $U_{LO} = \pm 1V$.

Block diagrams for one channel electronics are shown in Fig. 10 (bottom), together with the induced BPM signals for two channels.

Signals were also recorded for several waveguide monitor positions transverse to the beam direction[4]. After accounting for different amplitude factors of the BPM channels - attenuation in nearly all components as well as gain in the electronics - the signal function S_x as defined in Section 3.2 was derived from a linear fit to the data as presented in Fig. 11. Here, S_x is plotted versus transverse beam position for a rough scan (stepwidth $\Delta x = 500$ μm) and a fine scan ($\Delta x = 50$ μm).

The results can be reasonably described and interpreted using the image charge model (continuous curves). The horizontal sensitivity derived from the fine scan results to $S_x = (5.27 \pm 0.14)$ dB/mm which is somewhat lower than the wire test bench value of (5.79 ± 0.04) dB/mm. This can be explained by the fact that the beam size is larger than the linear region of the BPM, so that a fraction of the transverse beam profile laps into the saturation region of the monitor, which in turn lowers the signal expected. We have also compared the beam position in x, determined by using an algorithm developed for beam based calibration [12], with the set beam positions by the stepping motor and found linearity for off-sets up to about ± 2 mm with high precision.

[4]Steering along the vertical axis was not possible due to a system failure of one stepping monitor.

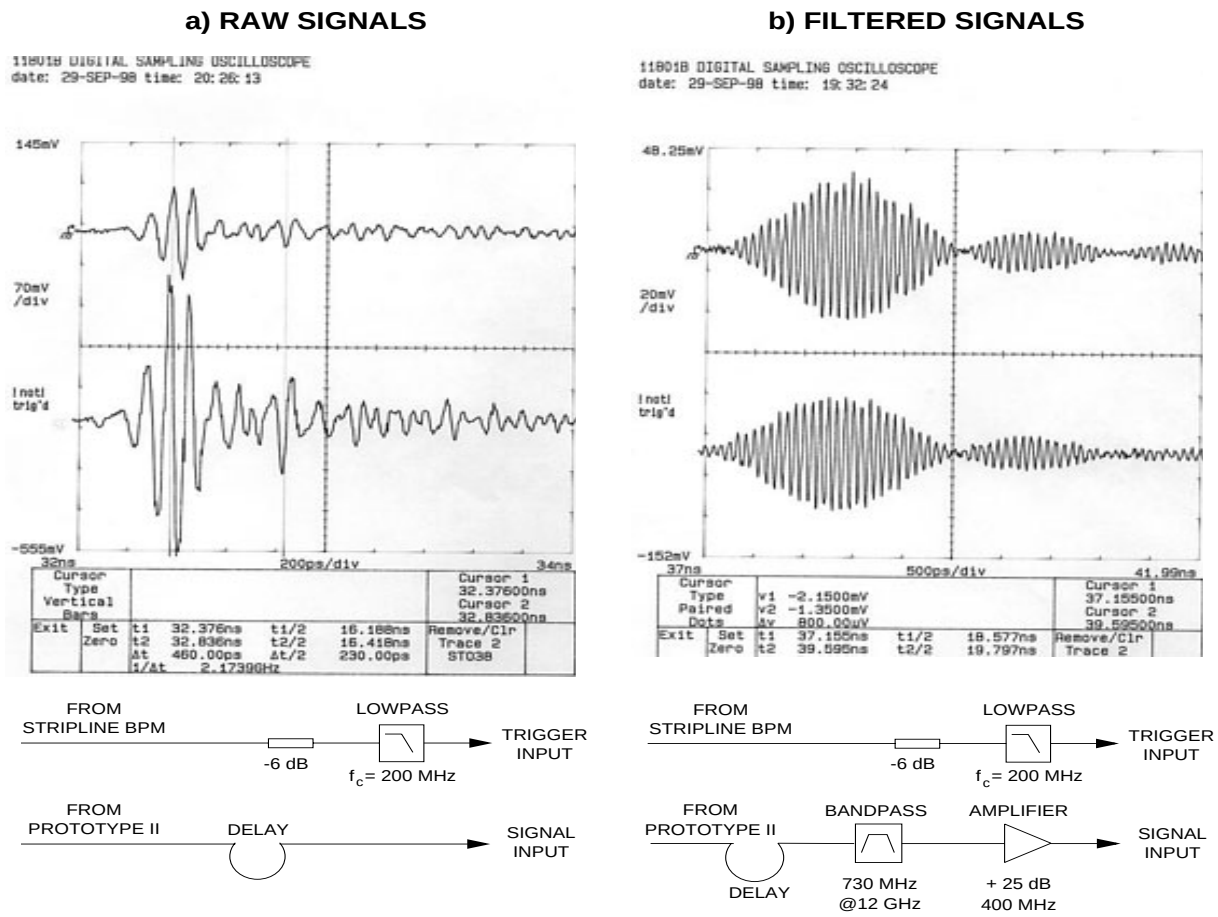

Figure 10: Measurements at the S-Band Test Facility: a) raw signals for two BPM channels, b) two 12 GHz filtered and amplified BPM signals. Bottom: block diagrams for one channel electronics.

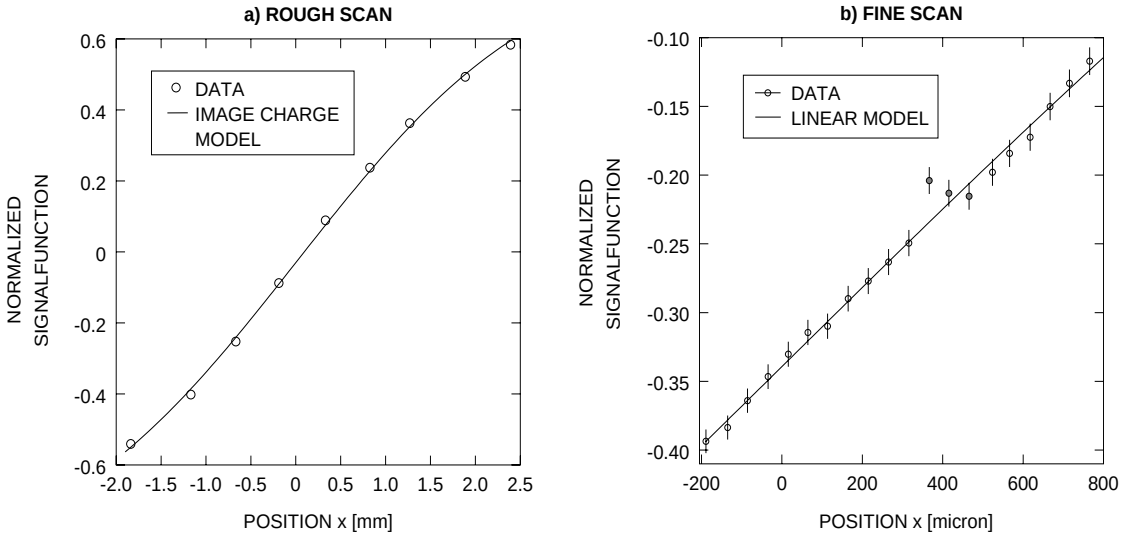

Figure 11: Relative signalfunction S_x for the horizontal plane: left) for a broad scan width of $\Delta x = 500\mu m$; right) for a narrow scan with $\Delta x = 50\mu m$. Three values around 400μm were excluded from the fit because of strong beam position jitter.

All measurements at the S-Band Test Facility were however limited by the granularity of the internal ADC of the oscilloscope. For operation at the TTF FEL an ADC was developed for optimum pulse response with significant better resolution (see section 5).

5 TTF FEL Measurements

For phase 1 of the TTF FEL the undulator [13] was segmented into three sections. The vacuum chamber of the third section was equipped with ten microwave monitors as an integrated part of the chamber. The vacuum chamber is a flat 4.5 m long structure with the cross section of 11.5×128 mm^2 of extruded aluminium, with a central aperture of 9.5 mm to guide the electron beam. In order to guarantee a tough control of the beam orbit inside the undulator one BPM and correction coil were required per FODO quadrupole of the undulator magnet structure. The correction coils were located in between the BPMs and allowed for horizontal and vertical steering of the beam. The waveguide holes with their relative complex contours and the small coupling slots at the beam aperture were fabricated by EDM. At the end of each waveguide a coaxial adapter with a special UHV compatible RF feedhrough was flange-mounted. The design of the Prototype II BPM is used for the TTF FEL monitors since exhaustive laboratory and beam tests have proven its functionality.

There occured however some problems during manufacturing and installation of the monitors so that two BPMs could not be used for measurements:

- due to unexpected deviations of the central hole during the extrusion of the undulator vacuum chamber two microwave channels were machined through to the beam pipe without forming a defined coupling slot
- after installation of the 40 microwave channels, two had missing electrical contact between RF feedthrough and waveguide.

Special mounting, alignment and support systems for the flat and long vacuum chamber allowed for a proper insertion of the chamber in the undulator gap and its positioning within a tenth of a millimeter in vertical and horizontal direction.

5.1 The Signal Processing Electronics

The signal processing electronics have been devided into two parts. The first part was a 12-to-1 GHz down-converter followed by a 1 GHz amplitude demodulator before the signals were sent to the analog-to-digital converter (ADC).

The four signals of a monitor were grouped together into one electronic box, housing the down-converter circuit. The ten boxes of all monitors were positioned close to the vacuum chamber, so that signal attenuation was minimized. After passing semi-rigid cables of about 1 to 2 m length, the signals from each BPM were processed within the down-converter in a parallel way by four identical hardware chains. A simplified one-channel block diagram of the down-converter electronics is shown in Fig. 12a.

The broadband monitor signal was filtered by a bandpass as the first active element within the chain, with a frequency of 12.0 GHz and a bandwidth of $\pm$70 MHz. This bandpass filter was designed as a 5-pole interdigital filter to suppress by more than 70 dB unwanted freqencies. A 20 dB directional coupler before this filter allowed to introduce an 8 dB 12.3 GHz reference signal for calibration purposes. This coupler was intended to monitor and compensate electronics drift during data taking. The necessary generator stabilized with a dielectrical resonator was also

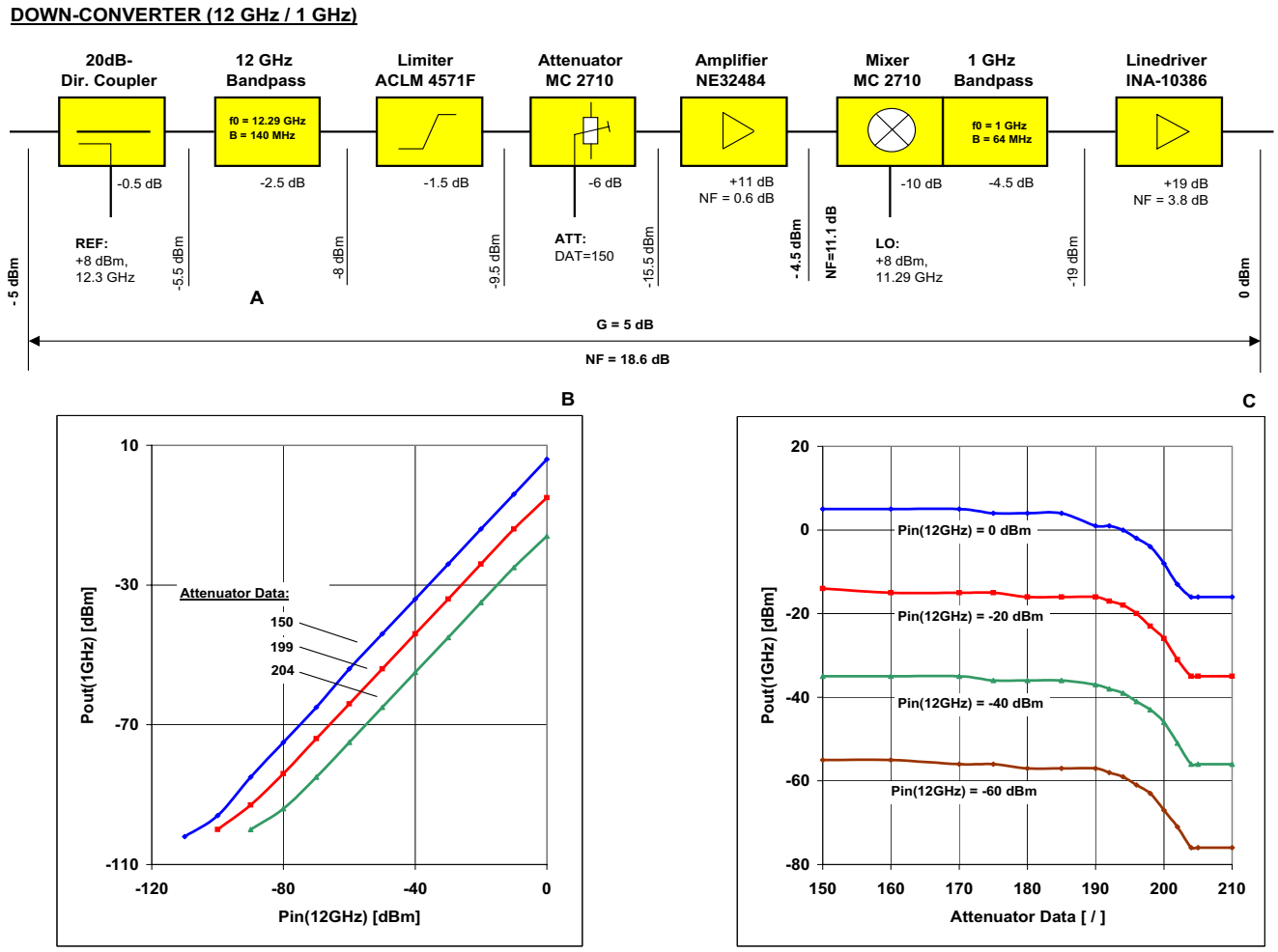

Figure 12: a) Block scheme for the 12-to-1 GHz down-converter electronics; b) Signal power transfer characteristics, P_{out} vs. P_{in}, for three attenuations; c) Output power P_{out} against attenuation for four input power values.

integrated into the down-converter box. Its on-off switching was realized by means of the I^2C remote control system.

After the 12 GHz bandpass filter a limiter (ACLM 4571F) protected the subsequent components from signal levels above some certain threshold, which might be caused by e.g. large mis-steering of the beam.

The limiter is followed by a combination of an attenuator and an amplifier intended to avoid saturation in the down-converter circuit as well as ensured an acceptable signal-to-noise ratio. For that, a symmetric 12 GHz mixer (MC 2710) steered by current regulation as an attenuator was combined with the microwave transistor NE32484 whose 1 dB-compression-point exists at 8.5 dBm. The actual attenuation level was set via the I^2C remote control system. In this way, the signal level was adjusted to -5 dB $\pm$10 dB.

The 12-to-1 GHz down-conversion was realized within a combination of the mixer MC2710 and a 1 GHz bandpass filter. The 8 dBm local oscillator signal of 11.3 GHz needed for the frequency down-conversion was generated by a circuit identical to the generator of the directional coupler. The stability of the local oscillator was $\sim$1 MHz. After amplification of the output signal by about 20 dB and some adjustments the signal was passed to the demodulator in the racks

outside the tunnel via a 50 Ω coaxial cable with a length of about 25 m. At this last stage of the converter the signal level was adjusted between -10 dBm and 0 dBm and had a width of ∼5 ns. The whole down-converter module was designed to have a total gain of about +5 dB with a Noise Figure of 20 dB.

Some characteristics of this module of the electronics are presented in Figs. 12b and 12c. At first, the overall signal power transfer characteristics, P_{out} versus P_{in}, is shown for three attenuation values. Fig. 12c shows the output power P_{out} as a function of attenuation for four discrete 12 GHz input power values.

Next, the down-converted 1 GHz signals were processed by amplitude demodulation. The simplest asynchronous (diode) demodulation was realized, on the cost of a relatively small linear range of the demodulator transfer function[5].

The simplified block diagram of the demodulator for one BPM channel is shown in Fig. 13a. The first two circuits represent a variable amplifier with a range of 13 dB ±9 dB, so that an optimal signal level for the ADC input range can be adapted. The amplitude-modulated signal is then detected (BAT14/03W) and filtered by a 25 MHz bandpass. At the end, the demodulated pulse was once more amplified and passed to the ADC. The four channels of a single BPM were grouped together and installed in a VME-RF cassette.

In Fig. 13b we present the output power of the demodulator before the detector BAT14/03W as a function of attenuation for three input power values. Fig. 13c shows for four channels of a BPM the output voltages V_{out} versus their input values V_{in} of the complete demodulator module. Linearity of the transfer function is indicated above -20 dB of V_{in}.

The final demodulator signal with a width of ∼25 ns has to be as jitter-free as possible and bunch-synchronized transferred to the ADC. Fig. 14a shows an example of such a simulated signal, with 872 mV peak-to-peak. The top region of the signal has been zoomed in Fig. 14b, from which the response of it convoluted with total noise is visible. With a noise rms of about 6 mV, the beam displacement resolution caused by signal processing electronics only was estimated to be about 12 μm. It is also worth mentioning that noise expected from the demodulator alone (without any input signal) was measured to about 300 μV rms and hence negligible compared to the overall noise level.

We remind that three signal attenuation possibilities for dynamic range optimization in the electronics were realized: i) at the entrance of the 12-to-1 GHz down-converter any attenuation was intended, ii) before the down-converter 12 GHz amplifier with maximum attenuation of 20 dB and iii) at the entrance of the demodulator, again with maximum attenuation of 20 dB. These possibilities were introduced to adjust the small dynamic range of the demodulator. Careful signal attenuation tuning is therefore required during data taking in order to obtain undisturbed pulses. In principle, an extension of the dynamic range of the electronics is possible by means of software correction procedures which have to rely on the transfer characteristics of each BPM channel.

The signals from the analog electronics were fed into an 8-channel high speed ADC with a resolution of 14 bit. It converted the signals with a rate of 1 MSample/s and stored the data in a SRAM memory on board with a depth of 128 kSample/channel [15]. The ADC was triggered and clocked by the TTF timing system. In order to sample the signal at the peak the clock was adjusted using a digital delay integrated on the ADC board, with 5 ns step size. The input

[5]In a first attempt we applied an I/Q demodulation with the commercial circiut MAX2105, which involved controlled gain and a quadrature-demodulator. However, the obtained signals were very noisy so that the resulting signal-to-noise ratios allowed only for unacceptable monitor resolutions of about 100 μm or more [14].

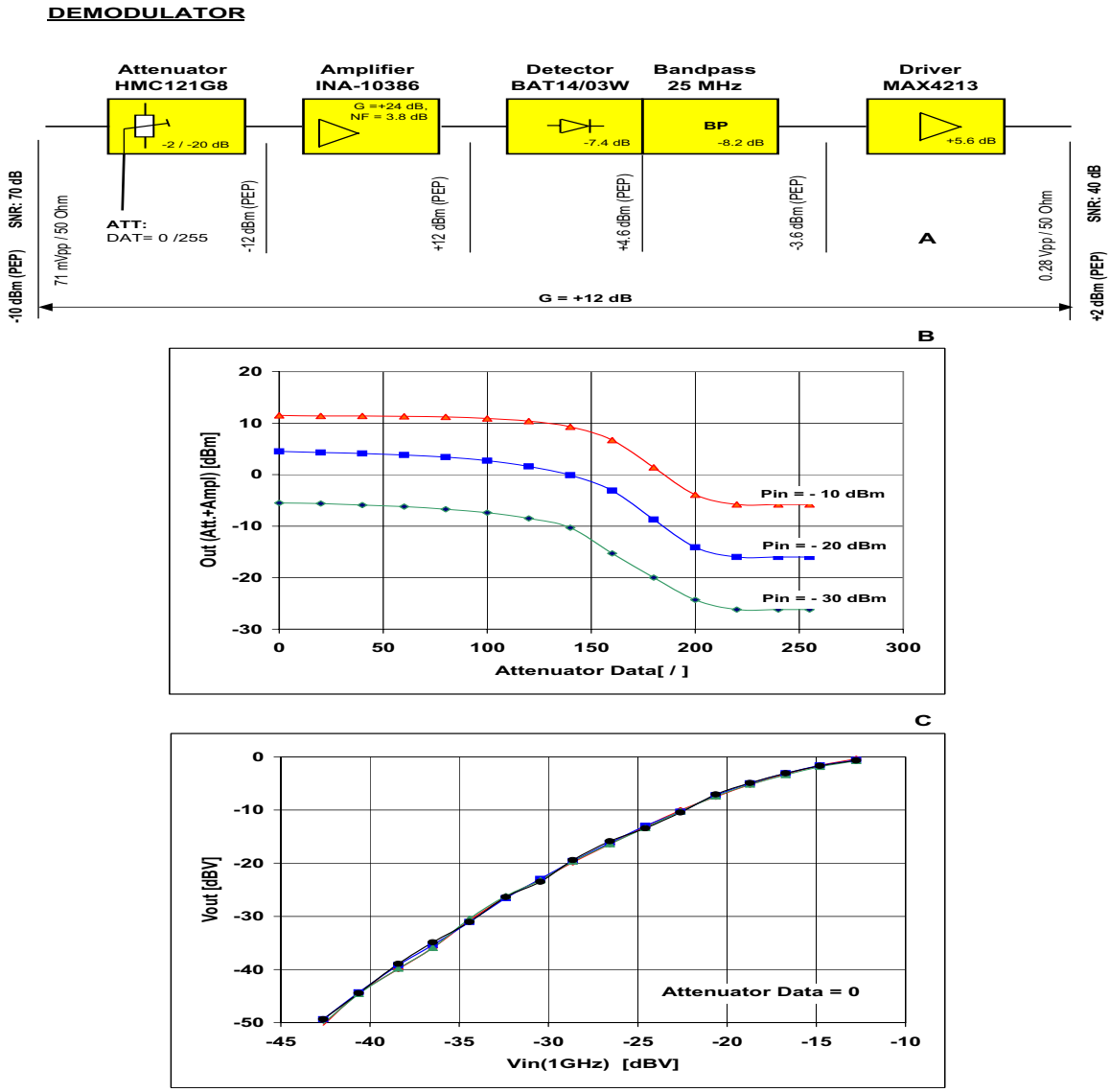

Figure 13: a) Block scheme of the demodulator electronics; b) Output power before the detector BAT14/03W against attenuation for three input power values; c) output voltages for four channels of a BPM versus input voltage V_{in} for the complete demodulator chain.

range of the ADC was set to ±1 V with an input impedance of 50 Ω. The ADC values were read out by the standard TTF data aquisition system.

5.2 Measurement Results

Measurements at the TTF FEL facility were performed to study the response of the monitors and their electronics as a whole system. Systematic studies were done for bunch charges of 0.5 to 5 nC at fixed beam position and for different beam displacements at a given beam intensity. Usually, the results presented were averaged over a sufficient number of individual bunches (typically 100) in order to avoid charge and position fluctuations during data taking. Data with extreme fluctuations (outliers) were rejected from the analysis. Tuning of the electronics by proper choices of mixer and amplifier attenuation respectively gain values for each BPM channel was needed to adjust the signals to the ∼(600±300) mV ADC input range.

The four signal voltages S_i (i=1...4) of a particular BPM are plotted in Fig. 15a as functions of the horizontal beam displacement achieved by different correction coil currents I_x, for a bunch

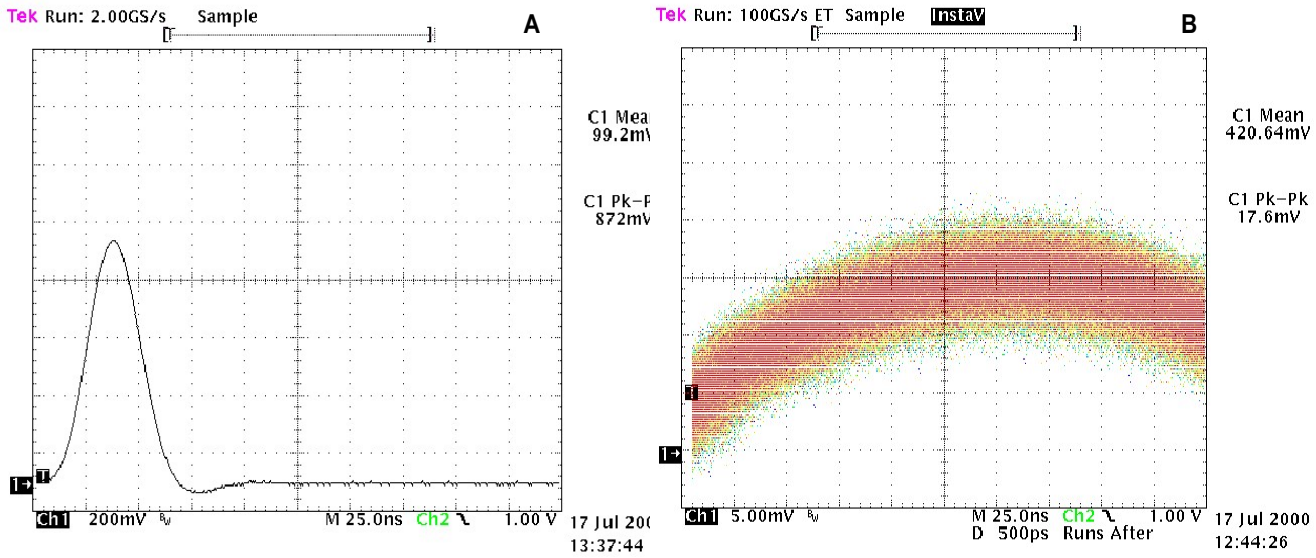

Figure 14: left) Typical voltage signal transferred to the ADC; right) Top region of the voltage signal zoomed.

charge of about 1 nC. The assignment of the signal notations to the waveguide channels can be taken from Fig. 7. Voltages S_1 and S_4 decrease with increasing I_x or off-sets in x direction, whereas S_2 and S_3 grow, in agreement with expectations. Fig. 15b shows the beam intensity defined as the sum of all four voltages against corrector current. The sudden change of the intensity near $I_x = 0$ is directly reflected to the voltage behaviour in Fig. 15a since the signals are directly proportional to the beam charge.

Quantities proportional to the beam displacement in horizontal and vertical directions are obtained by combining left/right and up/down signals

$$L = S_1 + S_4 \qquad R = S_2 + S_3$$

and

$$U = S_1 + S_2 \qquad D = S_3 + S_4$$

from which norm differences in x- and y-directions are derived:

$$F_x = (R - L)/(R + L) \qquad F_y = (U - D)/(U + D) \quad .$$

Another possibility to combine the four response functions relies by combining diagonal signals like

$$P = (S_1 - S_3)/(S_1 + S_3) \qquad S = (S_2 - S_4)/(S_2 + S_4)$$

to provide the skew differences

$$D_x = S - P \qquad D_y = S + P \quad .$$

Both, the norm and skew variables have the advantage of being independent of the bunch charge, so that beam intensity fluctuations cancel out. Figs. 15c and 15d show F_x and D_x, respectively, as functions of the steering current within ± 30 A which corresponds to beam

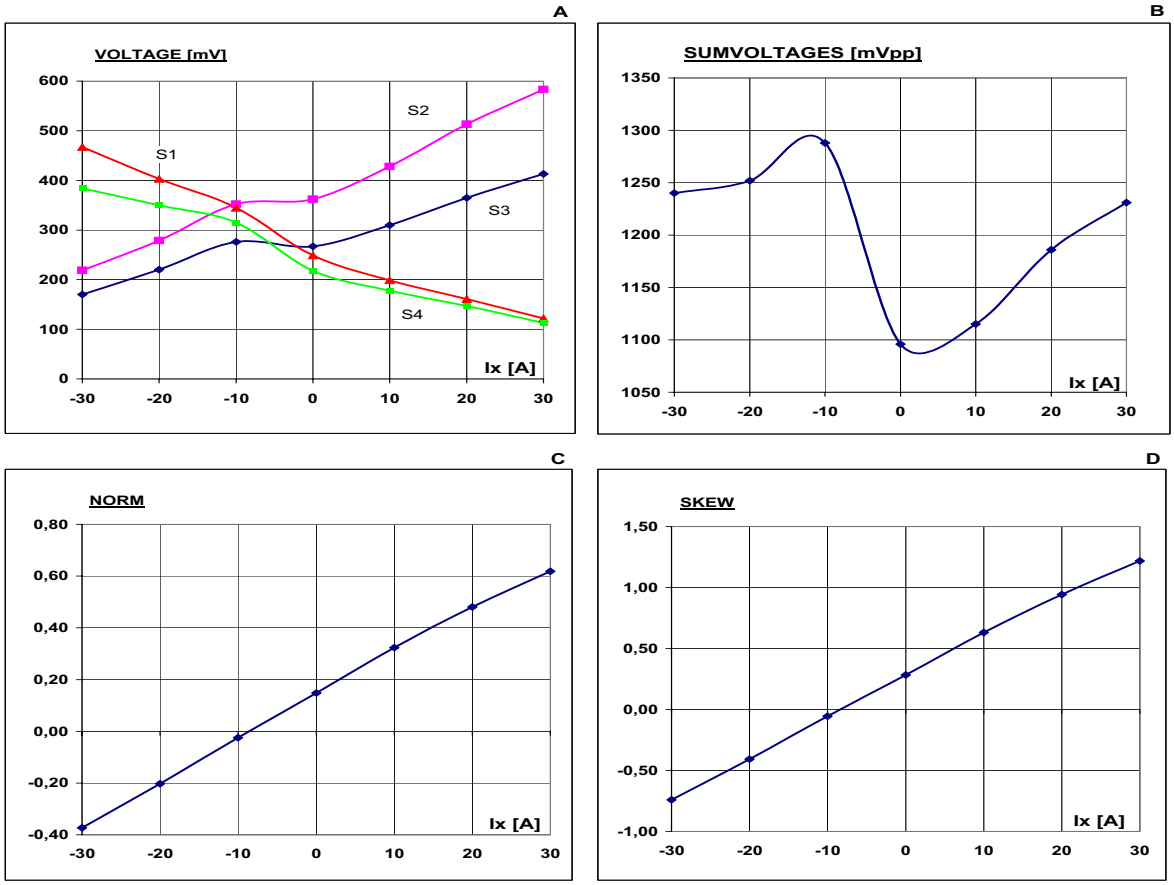

Figure 15: a) Signal voltages of a particular BPM against correction coil current; b) Beam intensity against correction coil current; c) Norm difference F_x and d) Skew difference D_x against correction coil current.

displacements in horizontal direction up to about ±1 mm. We observe an approximately linear behaviour of both quantities within this relatively large displacement range. It can also be noted that the slope of the skew difference D_x is larger, thus indicating a higher sensitivity against voltage fluctuations caused by either beam jitter or gain variations of signal processing elements and beam position. The same statement holds for the skew difference D_y.

In a further data taking period we determined the resolution of the BPMs. For that, the response of each monitor system was at first studied for e.g. 3.5 nC bunch charge with correction coil settings of the so called FEL mode. These settings were achieved to observe self-amplified spontaneous emission in a free-electron laser [3]. For this mode, the beam was believed to be positioned close to the center of the monitors and these positions define the point x = y = 0 in the following. After adjustment of the electronics gain and attenuator parameters, these settings were recorded for several bunch charges and had to be used during further measurements. For a given bunch charge, the beam was displaced in x and y in a controlled manner within each BPM[6]. Fig. 16 shows, as an example, the skew differences D_x and D_y for x (y) within ±1 (±0.5) mm for the second monitor in the vacuum chamber. In good approximation, a linear performance for both quantities is observed. In addition, the monitor also reveals a large robustness of D_x when y is modified and vice versa, D_y vs. x, as expected when D_x (D_y) is measured for beam steering in the y (x) direction.

[6]Changing the current in preselected correction coils and using a beam-based alignment procedure, predictions of relative beam positions within the BPMs are possible with high precision.

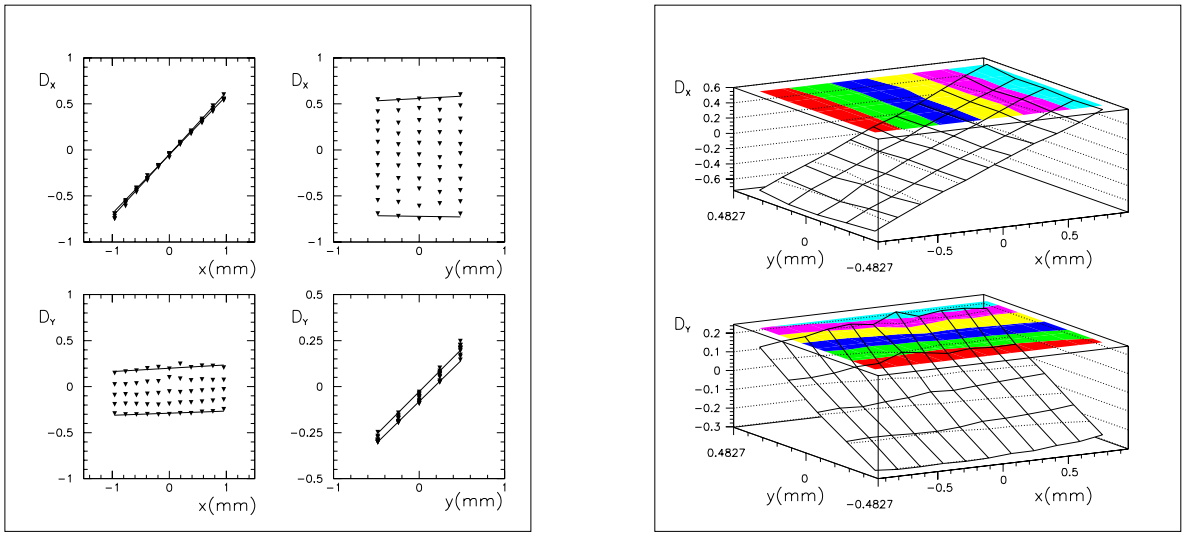

Figure 16: Skew differences D_x and D_y against beam displacements x and y (left) and the skew differences in the x-y plane (rigth).

Also, the sensitivity of the signalfunction in the horizontal direction is greater than in the vertical direction, as observed for the prototypes. This result is expected from the slot position differences within the BPM (see Fig. 1). Correlations of the skew differences might be deduced from Fig. 16 (right), where D_x and D_y are plotted as a function of the x-y displacement plane.

Typical 1-standard deviation errors for the skew differences D_x and D_y were found to be about 0.01. This together with the slope of the skew versus displacement variation results to the following upper limits for the beam position resolution of the waveguide monitors as installed into TTF FEL:

$$\Delta x < 25\ \mu m \qquad\qquad \Delta y < 30\ \mu m\ .$$

Since the beam-based alignment procedure predicts the beam position with an error of about 15 μm [16], the beam position resolution derived after deconvolution is in the order of the 12 μm uncertainty coming from the signal processing electronics.

The importance of selecting proper calibration values during data taking is demonstrated in Fig. 17. With the calibration data for 3.5 nC and a fixed beam position, D_x and D_y are shown as functions of the bunch charge between 0.5 and 3 nC. Clearly, both signalfunctions vary substantially up to 3 nC while charge independence would be expected. This result underlines the great sensitivity of the signal processing electronics on the setting parameters to ensure operation of the demodulation diodes within the linear range. Obviously, the dynamic range of at least one demodulator was exceeded during these measurements.

So far, all measurements were performed in a single-bunch regime, i.e. only one bunch with a 1 Hz repetition rate was accelerated and recorded. It is however intended to operate the accelerator e.g. at $\leq$10 Hz repetition rates with bunch trains of up to 7200 electron bunches into one bunch train [1]. Thus, measurements in a multi-bunch regime were needed to test the BPM and electronics under these conditions. The nominal bunch spacing during our multi-bunch operation was 1 μs, with 10 bunches within a train and a 1 Hz train repetition.

It has been found that with increasing bunch number (from 1 until 10) within a train the signal voltages decreased continously, roughly exponentially to about 80 % of the first bunch.

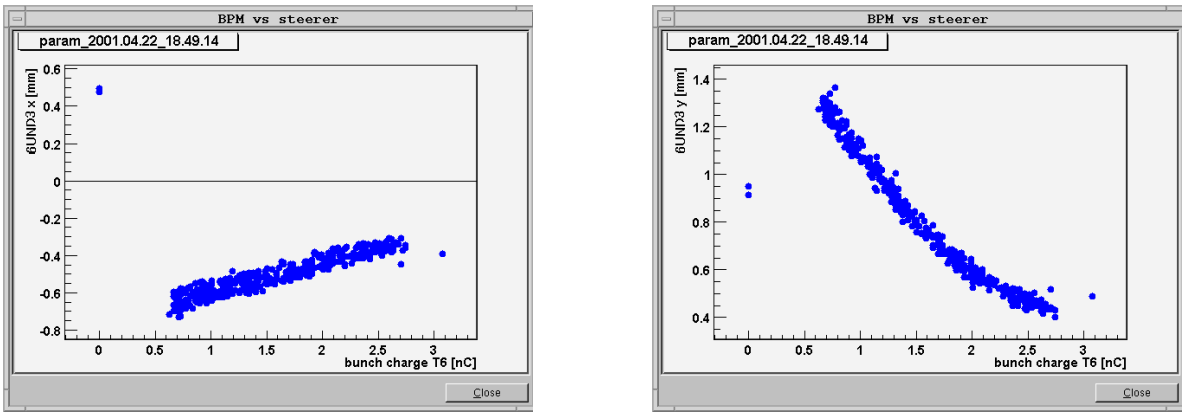

Figure 17: Skew differences D_x (left) and D_y (right) versus bunch charge.

Possible reasons for such a behaviour were searched for, with the conclusion that neither the ADC nor the BPM was responsible for such a pile-up effect. The design of the demodulator bandwidth of about 25 MHz should ensure pulse decays within 110 ns below 1% of its original maximum. Also, measurements of signal degradation within the demodulator module were performed with pulses of 10 μs spacing. No pile-up effect was observed. At the moment, the reason of this effect remains open and calls for new systematic data taking with carefully selected calibration values.

Fig. 18 shows the skew difference D_x for two bunch charges in dependence of the number of consecutive bunches (1-10) within a train, with correction coil currents set to the FEL values. Since the skew variables cancel out the bunch charge and hence any (also faked) variation of it, the small scattering visible around the zero-line might be ascribed to genuine bunch-to-bunch displacements (beam jitter). The variation of D_x typically smaller than 0.002 can be translated to an horizontal beam off-set scattering of $\lesssim$14 μm. This is consistent with expectations for local bunch-to-bunch fluctuations. However, this conclusion is not stringent due to possible non-linear dynamic range and/or signal time dependent effects of the analog electronics.

6 Improvements for Further Measurements

Measurements discussed in the previous section clearly underlined the importance of a large dynamic range of the signal processing electronics. It was also realized to be difficult for a TTF operator to adjust proper bunch charge dependent gain and attenuation values during data taking in order to record undisturbed signals of the BPMs within about $\pm$1 mm displacements. In principle, computer guided adjustments are possible if calibration files would exist for several bunch charges. The storage of such data requires however careful and time consuming measurements. Usually, such an approach is not practicable during first data taking periods aimed to study the reliability of a new BPM system.

Improved electronics with significantly larger dynamic range of the transfer characteristics would also enhance the monitor performance. According to our experience, we suggest to keep the division of the whole processing line into two parts, a 12-to-1 down-converter and a demodulator, with the down-converter as described in Section 5.1 unchanged. For the demodulator module improvements are highly desirable. A synchronous demodulation requires a precise time-independent phase relation between the beam signal and the LO signal. Due to possible time delays within the machine or modifications of signal transfer cables additional phase stabilization or phase adjustments are needed. A quadrature demodulator avoids a priori any phase synchronisation inherent of the synchronous demodulation and is recommended for the future.

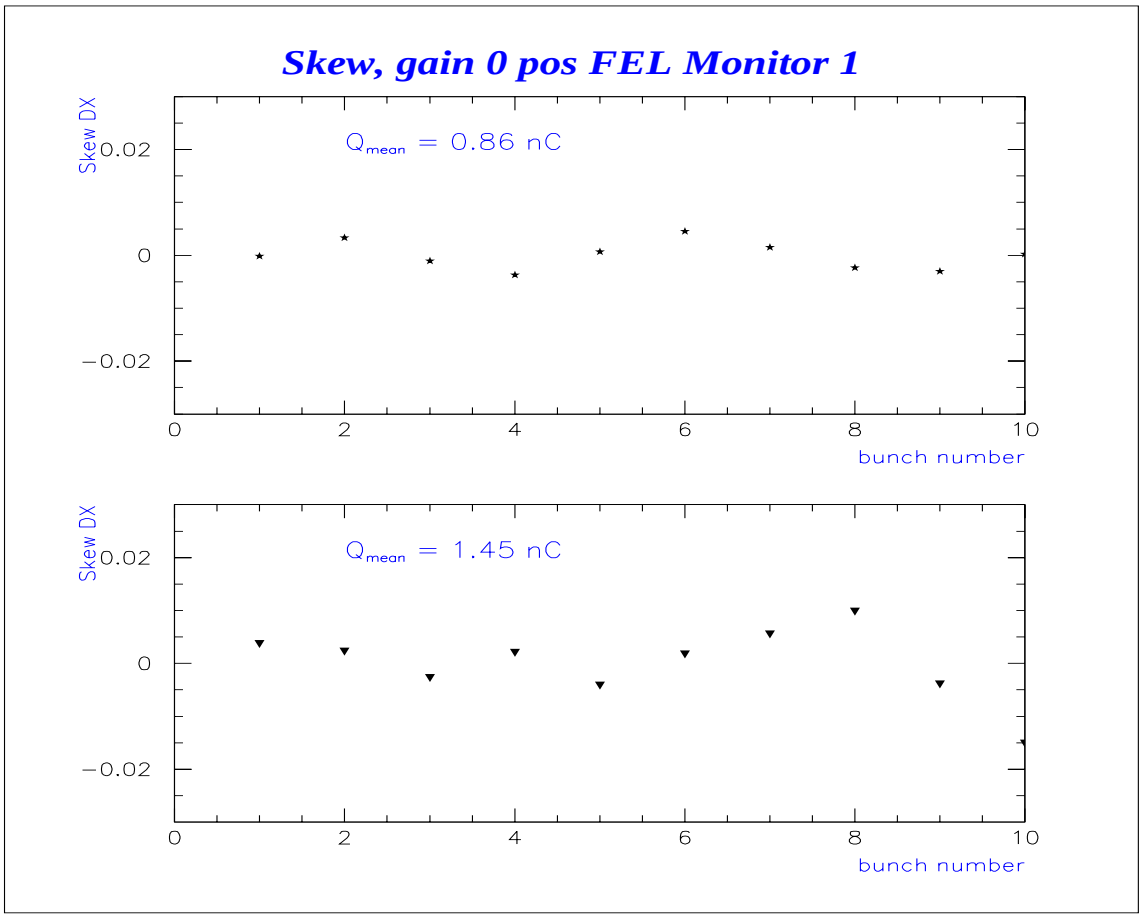

Figure 18: Skew difference D_x against the bunch number within a train, for two bunch charges.

In order to achieve few micrometer beam position resolution, this new demodulator has to have a noise level about 20 times lower than the I/Q demodulator of our first electronics (see Section 5.1).

Ideally, one would replace the demodulator components in Fig. 13a by a complex I/Q demodulator curcuit which contains an adjustable amplifier, a mixer and the demodulator itself with an appropriate signal-to-noise ratio. Searches revealed that such a curcuit was not commercially available. Thus, one should pursue to get individual components as commercial products and control the noise level below a predefined threshold.

7 Conclusions

The operation principle and the design of a waveguide BPM based on coupling to the electromagnetic field co-propagating with the electron beam has been presented and investigated. The waveguide concept relies on four waveguides with small slots arranged around the beam path. In order to fit in the narrow undulator vacuum chamber special ridged waveguides were designed which realize a sufficient high coupling amplitude. For each BPM, a set of waveguides and slots were split into two symmetric pairs separated by 40 mm along the beam direction. Each pair was positioned at $\pm 35^o$ with respect to the horizontal plane. According to MAFIA calculations the coupling factor of a single slot was about 1% at 12 GHz. At the end of the waveguide, the electromagnetic waves are transferred to a coaxial ultra-high vacuum feedthrough which is metallic sealed against the chamber body.

Two BPM prototypes were manufactured and exhaustively tested in a laboratory test bench

and with beam. It was found that the RF-characteristics were in agreement with expectations from theory. For laboratory tests, the prototype chambers were mounted on a precision stage and excited by a continuous RF signal on a streched wire simulating the electron beam. By moving the wire with respect to the BPM, beam position scans were performed.

Several reasons led us to conclude to continue with Prototype II:

- better broadband transition between waveguide and feedthrough,
- higher mechanical machining precision,
- better electrical contact of the waveguide and
- easy installation of the single monitor.

Results on transfer characteristics, gain factors and sensitivities obtained from laboratory and beam measurements were in good agreement with MAFIA simulations and the image charge model. They encouraged us to use the Prototype II design for waveguide monitors in one undulator module at the TTF FEL.

Ten waveguide BPMs were installed into the third vacuum chamber. The results obtained are summarized as follows:

- measurements performed after careful gain and attenuation adjustments revealed good linearity of the norm and skew differences, quantities proportional to the beam displacement, within a range of about ± 1 mm,
- beam position resolutions were determined to $\Delta x < 25$ μm and $\Delta y < 30$ μm,
- after deconvolution of the uncertainty of the predicted beam position from a beam-based alignment procedure, the resolution was estimated to be close to 12 μm,
- the 12-to-1 GHz down-converter met the requirements of the Noise Figure and sufficiently large dynamic range,
- a relatively small linear range of the demodulator transfer characteristics was observed.

Possible improvements of the waveguide BPM system are:

- application of an I/Q demodulator which together with sufficiently low noise would allow for few micrometer beam position resolution, also for multi-bunch operation,
- a significantly larger dynamic range of the demodulator would resolve the signal variation for bunches in a bunch train.

A high-precision beam position monitor based on a new microwave concept has proven its functionality. By improving the signal processing electronics as proposed the new BPM system would be an usable device for exact beam position measurements. This monitor type has a large potential for beam position monitoring in cases of extremely short electron bunches ($\lesssim$50 μm) at restricted space conditions in an accelerator.

Acknowledgments

The authors would like to express their gratitude to P. Castro, H. Henke, M. Sachwitz, G. Schmidt, R. Steinbrecher, H. Thom, K. Trützschler and M. Wendt for important contributions as well as valuable and encouraging discussions during different stages of the project.

References

[1] TESLA TEST FACILITY - Design Report, edited by D.A. Edwards, DESY Hamburg, TESLA-Note 95-01, March 1995;
SASE FEL at the TESLA Facility, Phase 2, TESLA-FEL 2002-01, June 2002;
A VUV Free Electron Laser at the TESLA Test Facility Linac - Conceptual Design Report, DESY Hamburg, TESLA-FEL 95-03, June 1995.

[2] for a review see e.g. TESLA Technical Design Report, DESY 2001-011, Part II, p.48 ff.

[3] J. Andruszkow et al., Phys. Rev. Letters 85 (2000) 3825.

[4] B. Faatz, J. Pflüger and Y.M. Nikitina, Nucl. Instr. and Meth. A393 (1997) 380.

[5] U. Hahn, P.K. den Hartog, J. Plüger, M. Rüter, G. Schmidt and E.M. Trakhtenberg, Nucl. Instr. and Meth. A445 (2000) 442.

[6] R. Klatt et al., MAFIA - A Three-Dimensional Electromagnetic CAD System for Magnets, RF Structures and Transient Wake-Fields Calculations, IEEE Proc. of the LINAC86 Conf., Geneva, Switzerland, 1986.

[7] T. Kamps, PhD Thesis, Humboldt University Berlin, 2000.

[8] M. Dohlus et al., TESLA-FEL-98-02, 1998.

[9] J.H. Cuperus, Nucl. Instr. and Meth. 145 (1977) 219.

[10] J.P. Dalahaye, The CLIC Study of a Multi-TeV e^+e^- Linear Collider, Proc. of the PAC99, New York, USA, 1999;
CLIC Team, CTF2 Design Report, CERN/PS-96-29, 1996.

[11] R. Brinkmann et al., Conceptual Design of a 500 GeV e^+e^- Linear Collider with Integrated X-ray Laser Facility, Vol. II, DESY 1997-048, ECFA 1997-182;
M. Schmitz, Status of the S-Band Test Facility, Proc. of the LC97, Zvenigorod, Russia, 1997.

[12] T. Kamps, Proc. of the FEL99 Conference, Hamburg, Germany, 1999.

[13] Y.M. Nikitina and J. Pflüger, Nucl. Instr. and Meth. A375 (1996) 3825.

[14] T. Kamps, W. Riesch and F. Tonisch, Proc. of the EPAC2000, Vienna, Austria, 2000.

[15] J. Andruszkow, P. Jurkiewicz and F. Tonisch, 8-channel FastADC with 14 bit resolution, `http://tesla.desy.de/doocs/hardware/8ch_10MHz_ADC_manuel.pdf`

[16] P. Castro, private communication.